Conical Diffuser Flows with Natural and Screen-Simulated Inlet Conditions

M. Sajben,* J.C. Kroutil,† and A.V. Sedrick‡
McDonnell Douglas Corporation, St. Louis, Mo.

Nonuniform screens are a practical method of simulating initial velocity distributions for the purpose of testing the performance of duct-like components of airbreathing propulsion systems. The degree of similarity between the flows obtained by using naturally developed inlet boundary layers and screen-generated profiles was investigated. Overall performance measurements were made in four moderate-area-ratio conical diffusers, each in connection with seven different axisymmetric, screen-generated inlet velocity profiles. The profiles simulated increasingly thicker turbulent boundary layers. The data were compared with published results relating to flows with natural inlet boundary layers. For the conditions investigated, screen simulation produced results acceptable for most engineering purposes.

Nomenclature

A = cross-sectional area
B = blockage, defined as $2\delta^*/R$
C_p = pressure coefficient for wall pressures, defined as $(p_w - p_{1w})/q_1$
C_{ps} = static pressure rise (recovery) coefficient, defined as $(p_2 - p_1)/q_1$
D = diameter
H = boundary-layer shape factor, defined as δ^*/θ
L = axial length of diffuser
M = Mach number
p = static pressure
q = dynamic pressure, defined as $\frac{1}{2}\bar{\rho}\bar{u}^2$
R = radius of cross section
Re_D = Reynolds number based on D_1 and $\bar{u}_1$
u = axial component of velocity vector
x = coordinate along diffuser axis. $x=0$ at beginning of area divergence and is positive in downstream direction
α = area ratio, defined as A_2/A_1
δ^* = displacement boundary-layer thickness, defined as

$$2u_{\max}^{-1} R^{-1} \int_0^R (1-u)\, rdr$$

ϕ = diffuser half-cone angle
ρ = density
ψ_x = defined in Eq. (2)
θ = boundary-layer momentum thickness, defined as

$$2u_{\max}^{-2} R^{-1} \int_0^R (1-u)\, rdr$$

η = effectiveness, defined as $C_{ps}/[1-(1/\alpha^2)]$

Subscripts

1,2 = inlet and exit stations, respectively
a = ambient
w = at wall
max = maximum over cross section
s = static
( ) = area average

Received March 22, 1976; revision received July 19, 1976. This research was conducted under the McDonnell Douglas Independent Research and Development Program.

Index category: Nozzle and Channel Flow.

*Senior Scientist, McDonnell Douglas Research Laboratories. Associate Fellow AIAA.

†Research Scientist, McDonnell Douglas Research Laboratories.

‡Research Scientist, McDonnell Douglas Research Laboratories. Member AIAA.

Introduction

IN the external flow problems of aeronautics, both upstream and downstream boundary conditions usually are defined as uniform, parallel flow, which is realized reasonably both in flight and in wind-tunnel conditions. In contrast, a duct-like component of an air breathing propulsion system may be forced to receive a large variety of profile shapes and turbulence structures. The exit conditions also may vary widely, involving a freejet, another duct com-

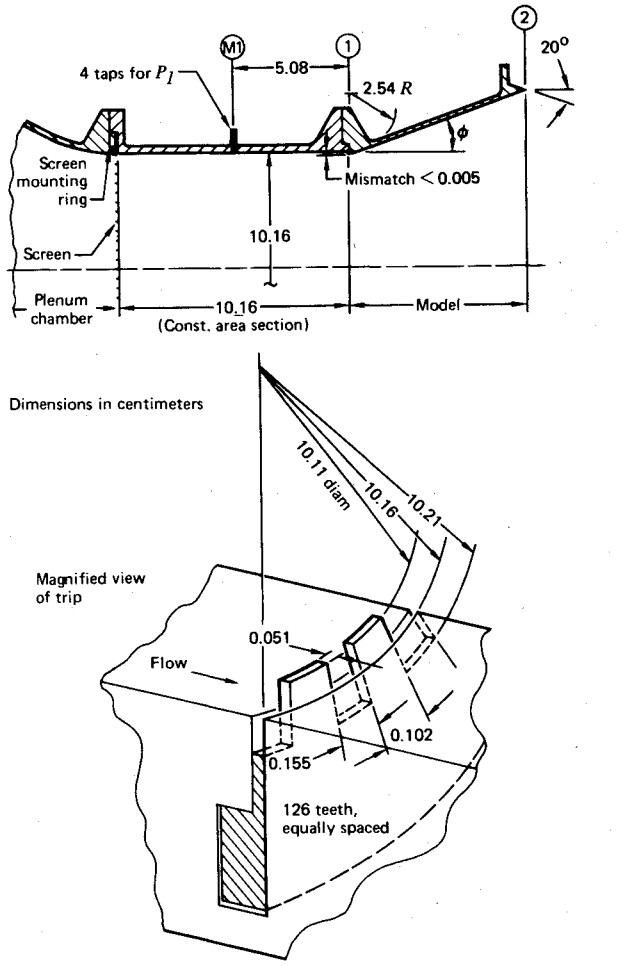

Fig. 1 Details of diffuser model mounted on test facility. Trip shown at bottom was used to generate profile 1.

ponent, a compressor, or a deflector of some sort. These conditions must be part of the problem specification, and their overwhelming importance to flows within relatively short ducts represents a difficulty foreign to the aerodynamics of external flows around bodies.[1]

It follows that realistic testing of propulsion system components (including the engine) requires the capability to produce a variety of inlet conditions. In order to meet this need, various methods for generating arbitrarily prescribed velocity profiles, using nonuniform or nonplanar screens, have been developed.[2-4]

The principal question concerning the use of such techniques is the quality of simulation attained, as measured by the degree of similarity between flows with natural and artificial inlet conditions. The purpose of this paper is to assess the extent of flow similarity by comparing experimentally obtained overall performance data for selected conical diffuser configurations, using both screen-produced and natural inlet conditions. The choice of diffusers as test cases is particularly appropriate for this comparison, because they are extremely sensitive to minor differences in inlet conditions; imperfect simulation therefore would cause sharp differences in overall performance.

Data with screen-produced inlet conditions were obtained and compared with data for naturally developed inlet boundary layers available from the literature. The comparison was based on two overall performance parameters: one is conventional effectiveness, which measures the static pressure rise in the diffuser for a given dynamic pressure at the entrance, and the other is flow nonuniformity at the diffuser exit, which is a quantity of prime interest in airbreathing propulsion. These parameters were determined for four conical diffusers, with seven different, axisymmetric inlet flow conditions in each. The data were examined for trends of dependence on model geometry and inlet flow conditions.

Test Techniques

Profile Generator Screens

A technique has been developed to generate axisymmetric but otherwise arbitrary velocity profiles using flat screens of nonuniform solidity. These screens are placed upstream of the inlet station of the diffuser as shown in Fig. 1. The screens are fabricated by electroplating a round piece of plain-weave, commercial screen while it is rotated about a horizontal axis, partially submerged in an electrolyte. Plating at a fixed immersion depth produces a characteristic radial distribution of deposit thickness. Arbitrary solidity distributions can be achieved by superimposing such elementary distributions. Details of the technique and the computations required to relate a prescribed velocity profile to a solidity distribution and eventually to a plating schedule are given in Ref. 2. The screens are mounted on a ring that is fitted between two flanges, one inlet diameter upstream of the diffuser inlet station. All screens were 10 wires/cm mesh size, with a 33% solidity before plating.

Distinction is made between the profile generated by the screen when followed by a constant-area pipe segment, and the velocity profile that exists when the screen is followed immediately by a model having streamwise variable cross sections. In subsonic flow, the model exerts an upstream influence, and the two profiles are not necessarily identical. In these experiments, the inlet profiles were measured at the exit of a one-radius-long, constant-area, sharp-edge nozzle.

The screen technique can generate a wide variety of profile shapes, which can be specified a priori. However, it does not necessarily reproduce the distributions of turbulence properties that exist in naturally developed boundary layers or duct flows, accentuating the question of whether such a simulation is of acceptable quality for engineering purposes. This problem is characteristic not only of the fabrication technique used here, but probably of other methods developed for the preparation of nonuniform screens.[5] The conclusions of this study therefore are relevant to most screen-type inlet flow conditioning devices.

Characterization of Diffuser Performance

A commonly employed diffuser performance parameter is the diffuser effectiveness η, defined here as

$$\frac{p_2 - p_1}{q_1 (1 - 1/\alpha^2)} \tag{1}$$

Since the diffusers exhausted to the laboratory, p_2 was taken to be the ambient pressure, and p_1 was the wall static pressure one radius upstream of the diffuser inlet, determined as the manifold average from four static pressure taps with even peripheral spacing.

The degree of distortion may be characterized without detailed flowfield measurements if the force sensed by the load cell in a static thrust stand is used to compute an appropriate index.[6] A coefficient can be defined with reference to any axial station as follows

$$\psi_x = \frac{1}{\bar{\rho} \bar{u}^2 A} \left[\int_A (p - p_a) \mathrm{d}A + \int_A \rho u^2 \mathrm{d}A \right] \tag{2}$$

The bracketed quantity is the impulse integrated over the cross-sectional area, and the denominator is a nominal impulse based on average velocity and density at the same station. If the model is attached to a thrust stand (as shown in Figs. 1 and 2), the force sensed by the load cell is equal to the bracketed quantity, as evaluated at the diffuser exit. Knowing the flowrate, stagnation conditions, and exit pressure, the average density and velocity also can be determined.

If the contribution from the first (pressure) integral is small (as usually is the case), then it is easily shown that

$$\psi_{x2} - 1 = \frac{1}{\bar{\rho}_2 \bar{u}_2^2 A_2} \int_{A_2} \rho (u - \bar{u})^2 \mathrm{d}A \tag{3}$$

Since the integrand is always positive, and increases as the deviation from uniformity increases, the coefficient ψ_{x2} can be used as an index describing the distortion at the diffuser exit. This index offers several advantages both from theoretical and experimental viewpoints, as elaborated in Ref. 4.

Detailed comparisons, reported earlier,[7] show that ψ_{x2} correlated well with a distortion index widely used in propulsion engineering practice.§ This correlation permits a valid comparison between the present data and much distortion information available from the literature.

Test Equipment

Test Facility

A schematic of the experimental facility is shown in Fig. 2. The basic element is a well-screened plenum chamber, used as a static thrust stand. The plenum is supported by three air bearings, which allow the chamber to move in the horizontal plane, restrained only by the three load cells shown. Only the axial load cell was used for the present measurements.

Filtered, dry air enters through two diagonally opposed inlet tubes of 22.9 cm diam. Compressed air is passed between the flanges of the (metric) plenum and the mating part of the support structure; thus, the metric break functions as an air bearing without solid-solid contact. Hysteresis of the system is due to load cells only. No-flow tare forces resulting from

§The index referred to is defined as the difference between maximum and minimum total pressures, divided by the average total pressure over the exit cross section. The definition is to be used with a particular configuration of total pressure probe rakes.

flange misalignment are of the order of 1%, highly repeatable, and correlated for in the data reduction process.

The entire static force measurement system is calibrated by applying known weights through a linkage by use of flexures of negligible stiffness. The scatter of force calibration points is less than 0.1% of full scale (110 N). Statham load cells were used (model UC3) to measure the forces.

The plenum chamber is followed by a carefully shaped contraction segment of 25:1 area ratio. No separation occurs within the contraction at any flowrate. The screens were mounted at the plenum exit, followed by a 10.2-cm-long constant area section (Fig. 1). The purpose of this section is to establish nearly parallel flow, and thereby a nearly uniform static pressure at the station (M1), where the inlet pressure p_I is measured. The static taps were 5.1 cm (1 rad) downstream of the screens.

Flowrate was measured with a choked flowmeter built into the air supply line (calibration was NBS traceable). Calibration data scatter was $\pm 0.2\%$ over a 10:1 Reynolds number range. Flowrates ranged up to 1.0 kg/sec, corresponding to a maximum Reynolds number (Re_D) of $\cong 700{,}000$ at the diffuser inlet. Inlet Mach numbers varied up to 0.3.

Mean velocities and turbulent intensities were measured with a Thermo Systems, Inc., model 1010A constant temperature hotfilm anemometer, using a model 1005B linearizer. A 25-μm-diam quartz hotfilm sensor was used, with low pass filtering at 10 kHz. Further details of the experimental equipment and procedures are given in Ref. 6.

Models

Four straight, conical diffuser shapes were selected for study: two with an area ratio of 1.64 and included cone angles of 8 and 12 deg, and two with an area ratio of 2.43 and included cone angles of 12 and 16 deg. Measured dimensions are given in Table 1. The wall contours of all four models had a 2.54-cm radius of curvature at their inlet. This curvature is related directly to the wall pressure gradients at the inlet, which in turn may have influenced significantly the behavior of the boundary layer further downstream.

All models had six static pressure taps along one generatrix of the cone, and six equally spaced taps at the last station, 1 cm upstream from the exit. The latter group served to detect deviations from axial symmetry. All taps were 0.36-mm i.d., with a 45°/0.08-mm chamfer.

One set of test runs was made with turbulent boundary layers generated by a trip inserted between the plenum and the 10.2-cm-long tube section. The trip had a serrated, three-dimensional shape as shown in Fig. 1.[8] Other inlet conditions were created by replacing the trip with various screens.

Inlet/Exit Conditions

Inlet Profiles

Seven different inlet velocity profiles were tested, as summarized in Table 2. Profiles 1 through 7 are in order of increasing displacement thickness, as measured 5.2 cm downstream of the screen by a hot-wire anemometer, without the model being attached.

If no inlet manipulator device is used, the boundary-layer profile has a nearly Blasius shape, because of laminarization in the large area ratio contraction. Turbulent fluctuations were nevertheless quite noticeable within the layer, indicating that laminarization was not complete. The variation of boundary-layer parameters with flowrate and the associated diffuser performance in this case have been documented in Ref. 6.

Table 1 Measured diffuser model dimensions

α	2ϕ (deg)	D_I (cm)	L (cm)	L/R_I	$1-\frac{1}{\alpha^2}$
1.632	7.91	10.152	20.52	4.043	0.625
1.636	12.09	10.173	13.54	2.662	0.626
2.427	12.02	10.147	27.10	5.342	0.830
2.440	16.06	10.160	20.42	4.020	0.832

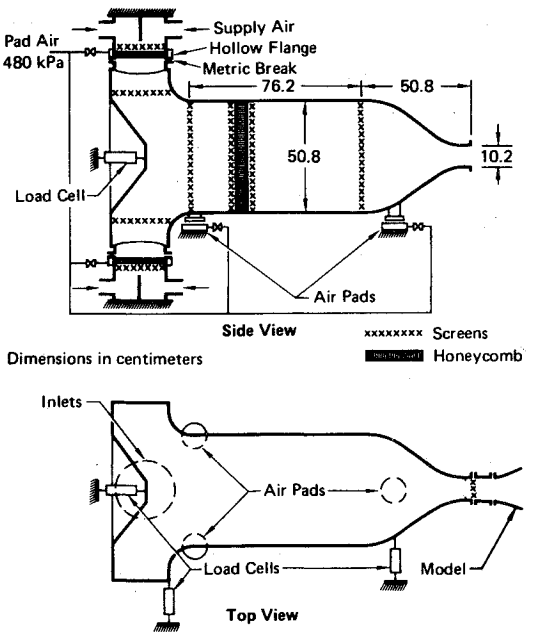

Fig. 2 Layout of test facility.

Profile 1 is generated by the serrated trip shown in Fig. 1. Representative profile shapes are shown in Fig. 3, and integral parameters are given in Fig. 4. Note that the trip is effective only for Reynolds numbers greater than 150,000.

Screen-generated profiles are shown in Fig. 5. Profile 2 is obtained by use of a uniform, unplated screen. The screen increases the core flow turbulent intensity threefold to 0.9%, but leaves the core flow velocity profile uniform. The boundary layer is slightly thickened by the screen-wall interaction, but it remains essentially thin as compared with the tube radius. The purpose of using this screen is to demonstrate that the diffuser performance changes caused by screens nos. 3-7 are attributable to the mean velocity profile shapes and not to alteration of the turbulence levels.

Profiles 3-6 simulate a systematic sequence of increasingly thicker turbulent boundary layers (at zero pressure gradient). The measured profiles are shown in Fig. 5. Continuous lines show the intended profiles used in the screen design process.

The turbulent intensity distributions are shown in Fig. 6. A characteristic of this screen technique is that these distributions cannot be prescribed—they are determined implicitly by the shape of the mean velocity profile. For comparison, the turbulence intensity distribution for a turbulent boundary layer in zero pressure gradient (from Ref. 9) is shown for profile 5, scaled for a boundary-layer thickness of $\delta = 0.55\ R$. Profile 6 simulates a fully developed pipe flow

Table 2 Inlet velocity profiles at $x/R = -1$

I.D. number	Method of generation	B_I at $Re_D \cong 430\,000$	Turbulence intensity on axis (%)
–	No manipulation (≈ approach profile)	0.012	0.3
1	Trip (Fig. 1)	0.014	0.3
2	Unplated uniform screen	0.028	0.9
3	Plated screen	0.059	0.9
4	Plated screen	0.068	0.9
5	Plated screen	0.103	0.9
6	Plated screen	0.164	0.8
7	Plated screen	0.244	0.7

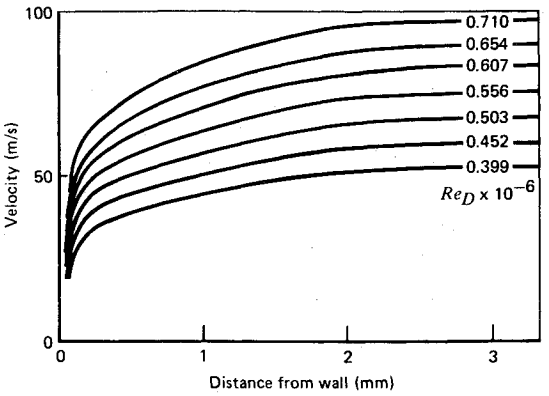

Fig. 3 Trip-generated boundary layer velocity profiles (no. 1), measured with a hot-wire anemometer, 5.20 cm downstream of screen.

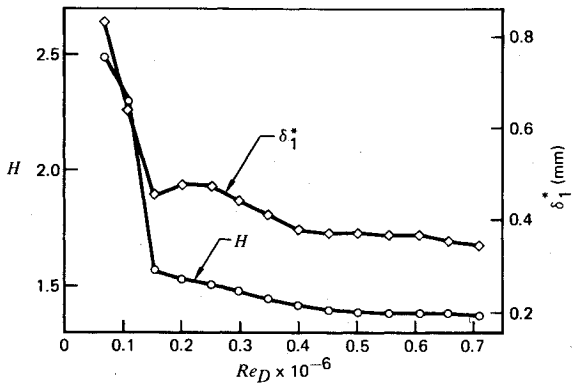

Fig. 4 Displacement boundary-layer thickness and shape factor for profile 1.

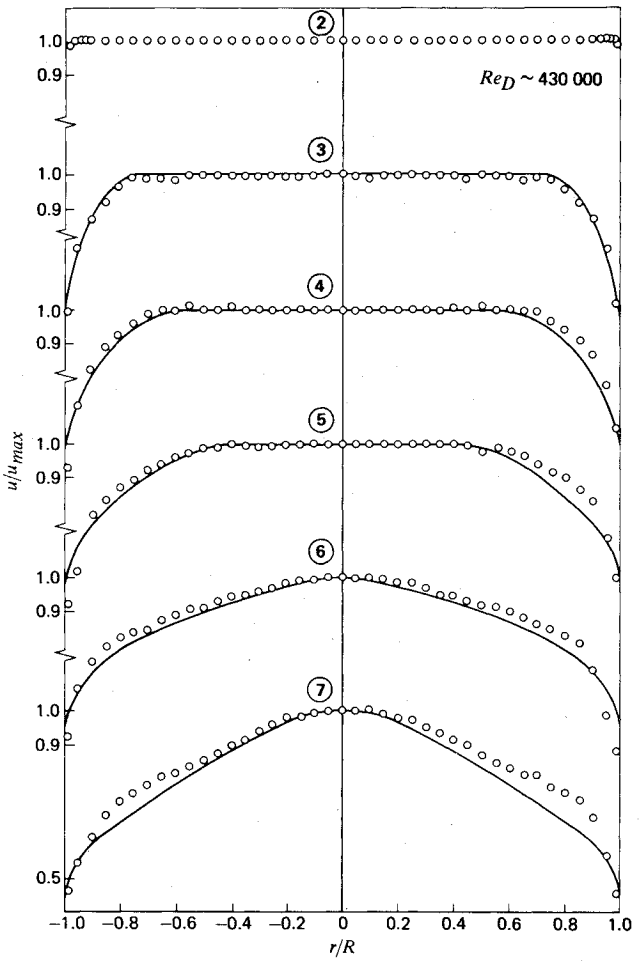

Fig. 5 Screen generated velocity profiles 5.20 cm downstream of screen. Solid lines show intended shape; symbols are hot-wire data. Profile parameters are given in Table 1.

profile. The turbulent intensity distribution present in naturally developed pipe flows, taken from Ref. 10, is shown by the continuous line. The screen-produced turbulence in both cases is less intense and more evenly distributed than the distributions in the respective naturally developed flows.

Profile 7 was obtained by increasing the wake component[11] of the intended turbulent boundary layer (of thickness $\delta = R$). The result is a shape similar to that at the exit of a long, small cone-angle diffuser.

Exit Conditions

The flow from the tested diffusers exhausted directly to the atmosphere. The exit static pressure used in computing C_{ps} was assumed to be equal to the ambient pressure. A mild radial pressure variation existed at this station such that the outer streamline was in fact close to atmospheric pressure, and the pressure on the axis was below ambient by approximately 5-8% of q_2. The C_{ps} values presented here are therefore slightly greater than those that would be obtained by use of area or mass-flow weighted average static pressures.

Experimental Results

Flowrate Effects on Overall Performance

Figures 7 and 8 show typical data obtained in the experiments. Effectiveness and exit distortion were measured at a number of flowrates in the (approximate) range of 0.2 to 1.0 kg/sec. The results are presented as functions of Reynolds number based on inlet diameter, although this choice of the independent variable is somewhat arbitrary; variation of flowrate implies concurrent variation of both Reynolds and Mach numbers. Typically, $M = 0.3$ when $Re_D = 700{,}000$, corresponding approximately to the highest available flowrate. Fortunately, both of these effects tend to increase η as the flowrate increases, which allows estimation of an upper limit for the combined influence. (This would not be possible if the effects tended to cancel each other.) Since the experimental evidence of Figs. 7 and 8 shows the net change to be small, each effect by itself must be small. Estimates further supporting this argument are presented in the following.

Mach numbers near 0.3 are sufficiently high to modify values of η considerably. If $(p_2 - p_1)/q_1$ is computed from one-dimensional, inviscid, incompressible theory, then η is predicted from Eq. (1) to be unity. Adding compressibility, however, causes η to be greater than one for a thermally and calorically perfect gas ($\gamma = 1.4$) as illustrated in Table 3, and reflected in the results of Fig. 7.

The parameter ψ_{x2} is defined in terms of flow properties at the exit station alone, so that its one-dimensional value is unity whether or not compressibility is considered. The effect of viscous forces is not estimated easily, but a slight performance improvement generally is expected with increasing Reynolds number. The weak Reynolds number dependence is well-documented in the diffuser literature.

In addition to viscous and compressibility effects, the shape of the inlet velocity profile also varies concurrently with the flowrate. This effect is probably the greatest for the no. 1 (trip generated) profile and also for the uniform screen (no. 2), in which the nonuniformities are confined to thicknesses comparable to those of the approaching boundary layer.

Screen-generated profiles (3-7) also were found to change with flowrate; in general they tend to be more flat at higher speeds. However, the changes were slight within the range of flowrates used, and therefore were not explicitly taken into account.

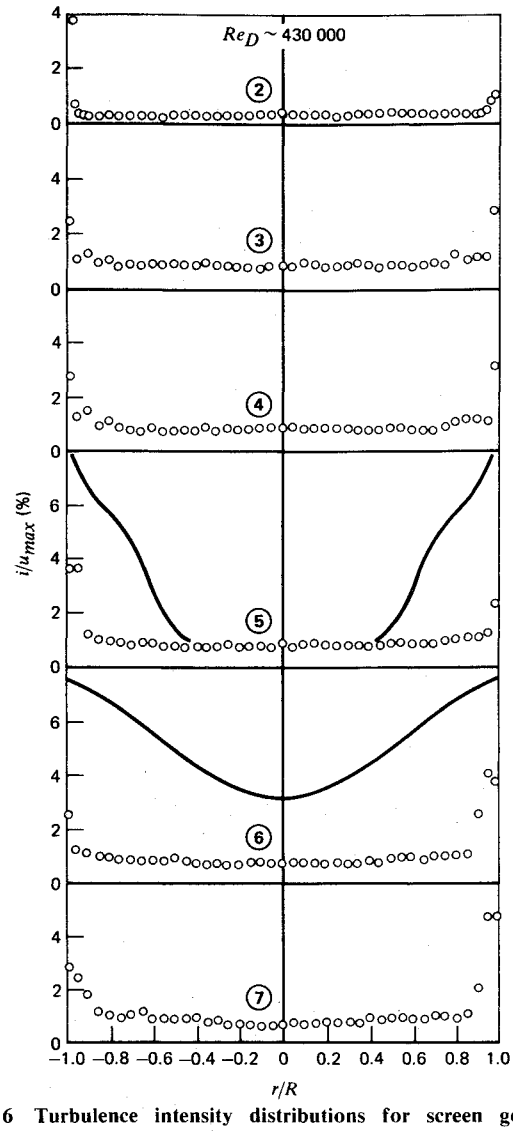

Fig. 6 Turbulence intensity distributions for screen generated profiles. Natural distributions are given for profiles 5 and 6.

The conclusion is drawn that the net result of viscosity, compressibility, and flowrate induced inlet profile shape changes is minor and need not be considered further. Data will be presented for the fixed Reynolds numbers of 430,000 and 215,000 unless otherwise noted.

Wall Pressure Distributions

Figure 9 shows a typical set of wall pressure distributions for the $\alpha = 2.43$, $2\phi = 12$ deg diffuser. The theoretical distribution for potential flow, obtained using a computer program by Hoffman,[12] also is shown for comparison.

The pressure distributions indicate that profiles 1 and 2 resulted in attached flow and a nearly inviscid pressure distribution. All other profiles resulted in separated flow, as verified by direct observation of tufts at the exit and as reflected in the measured wall pressure distributions. Inlet

Table 3 Effectiveness values from two-dimensional inviscid, compressible flow theory

α		M		
		0	0.15	0.3
1.30	η =	1.0	1.015	1.065
1.64		1.0	1.011	1.049
2.43		1.0	1.088	1.034

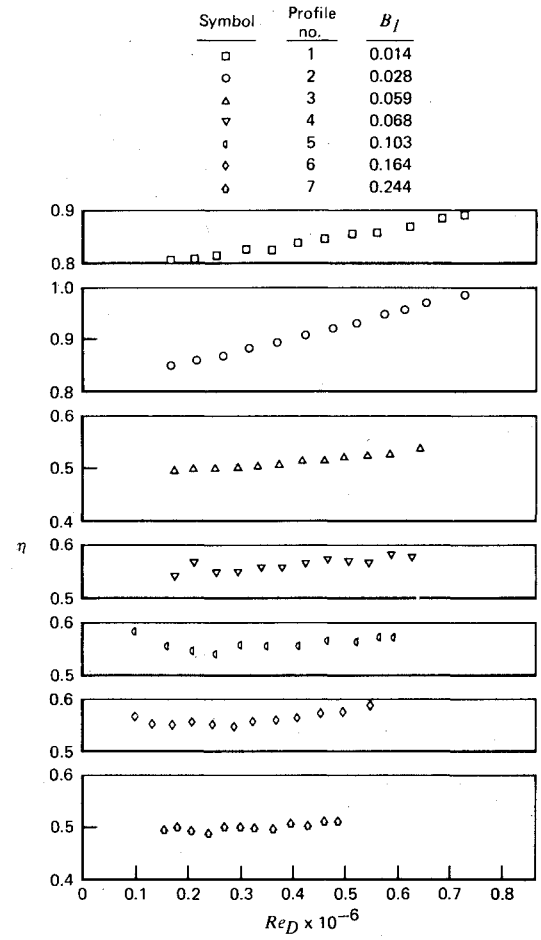

Fig. 7 Effectiveness as a function of Reynolds number for the 2.43/12 diffuser. Inlet profile data given in Table 2.

profiles 3–6 produced nearly identical wall pressure plots, indicating a relative insensitivity to B_I in the $B_I = 0.060$–0.16 range. Profile 7, however, shows a noticeably poorer performance, probably because of its peaked shape. The pressure at the first tap ($x/R = 0.23$) is conspicuously high. One possible explanation is that a small separation bubble exists at the throat, and the reattachment point is very close to this particular tap.

None of the pressure distributions extrapolate smoothly to the ambient, laboratory pressure; they are invariably below the ambient level by about 5–10% of the exit dynamic pressure. The reason for this is not clear; it may be due to a local depression of static pressure near the diffuser exit, caused by entrainment-induced secondary flow.

Inlet Blockage Influence on Distortion

Figure 10 shows the dependence of ψ_{x2} on inlet blockage for all diffuser models tested. Points representing runs with inlet screens are connected with straight-line segments for easier interpretation. The plots show the expected deterioration of performance as the boundary-layer thickness increases. Beyond approximately 10% blockage, further degradation of performance is minor, and some improvement is seen for the 2.43/12 diffuser. The performance with profile 7 clearly deviates from the trend established by the first five screens, quite possibly because the shape factor of the profile is different from the rest.

The flat screen (no. 2) slightly outperforms the trip-generated, thin turbulent boundary layer combined with a low turbulence core flow (no. 1). The reason may lie in the higher core flow turbulence, the beneficial effects of which have been demonstrated recently by Sharan.[13] Although his data were taken at much higher turbulence intensities (5–10%), our

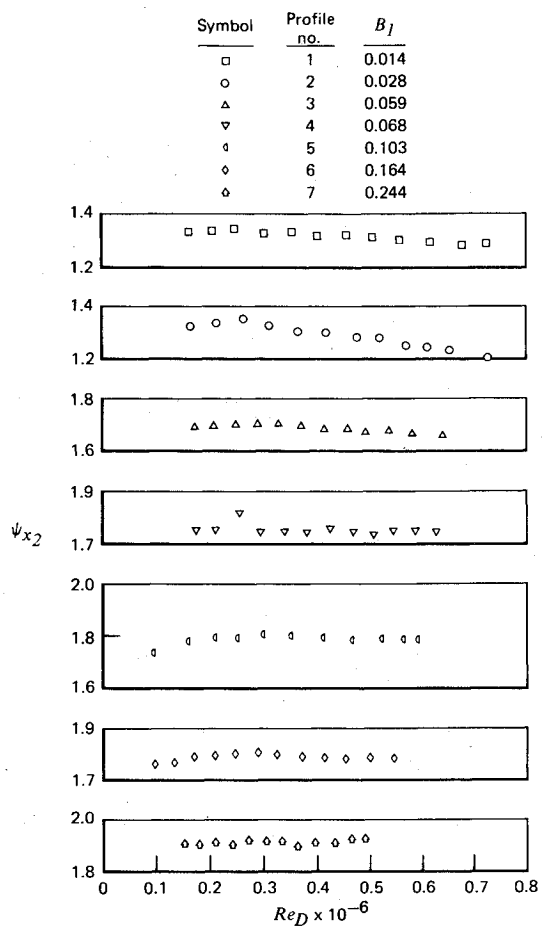

Fig. 8 Distortion index as a function of Reynolds number for the 2.43/12 diffuser. Inlet profile data given in Table 2.

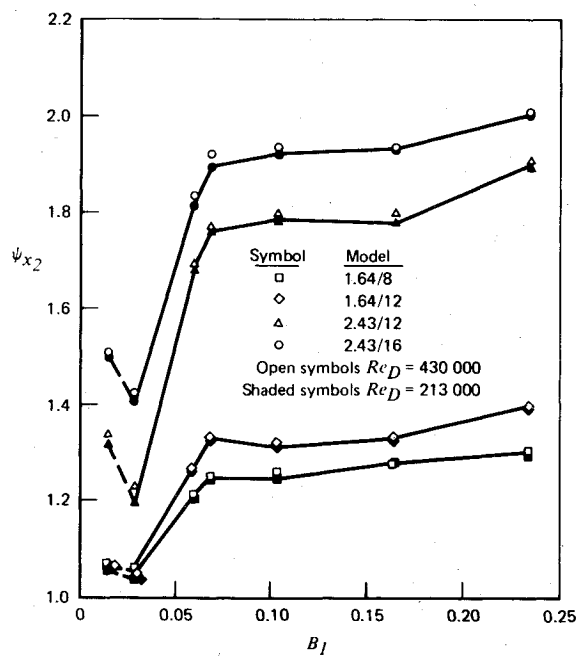

Fig. 10 Exit distortion as a function of inlet blockage.

results show that such an effect also may be present at quite low turbulence levels.

Comparison with Data Using Natural Inlet Conditions

Sixteen sources of conical diffuser data were examined for pertinent experimental information. Data were considered comparable if they satisfied all of the following requirements: 1) conical, straight diffusers; 2) $\alpha \leq 3$, $10° < 2\phi < 18°$; 3) $0 \leq M_1 \leq 0.35$; 4) $50{,}000 \leq Re_D \leq 1{,}500{,}000$; 5) inlet profile, or at

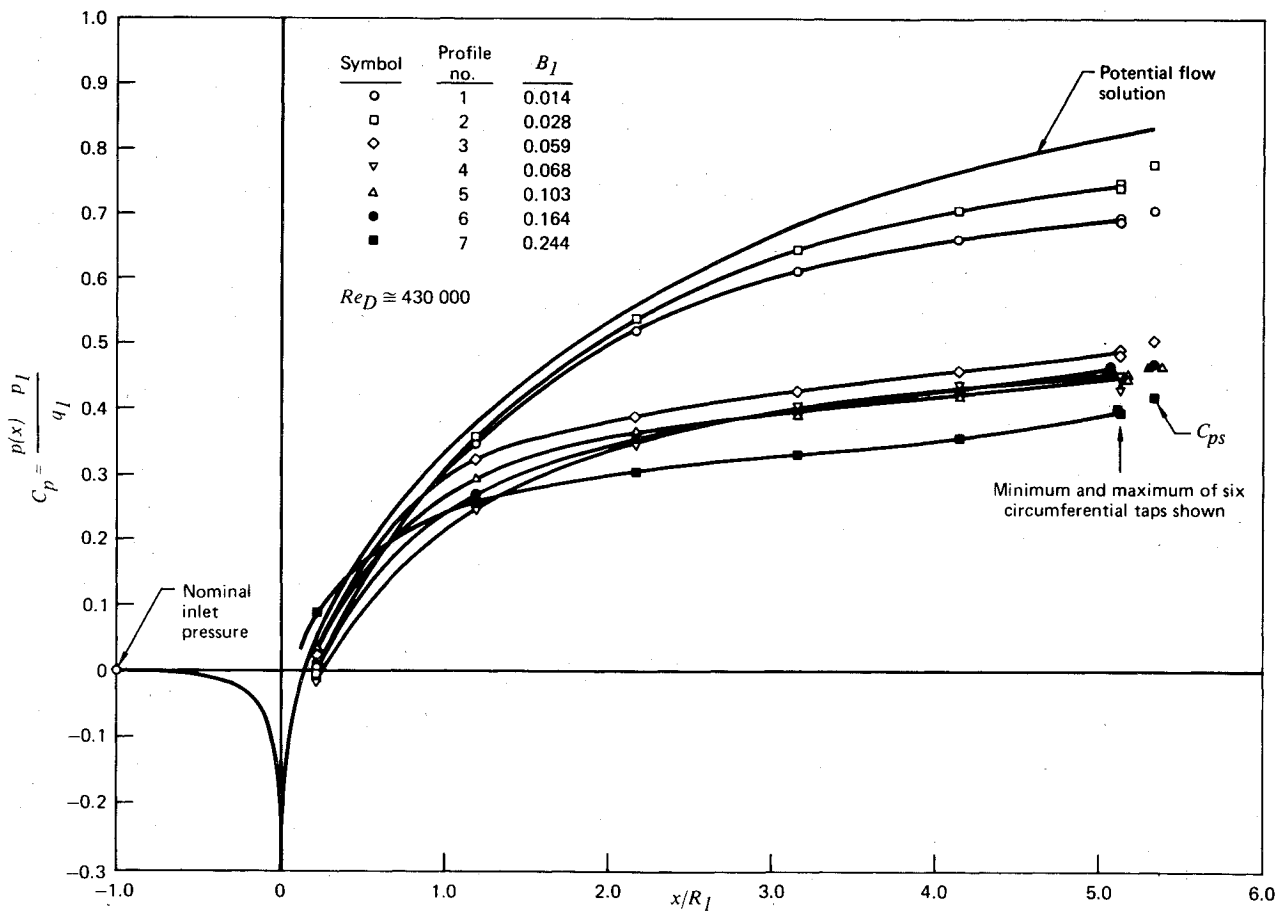

Fig. 9 Wall pressure distributions at various inlet blockage values in diffuser 2.43/12.

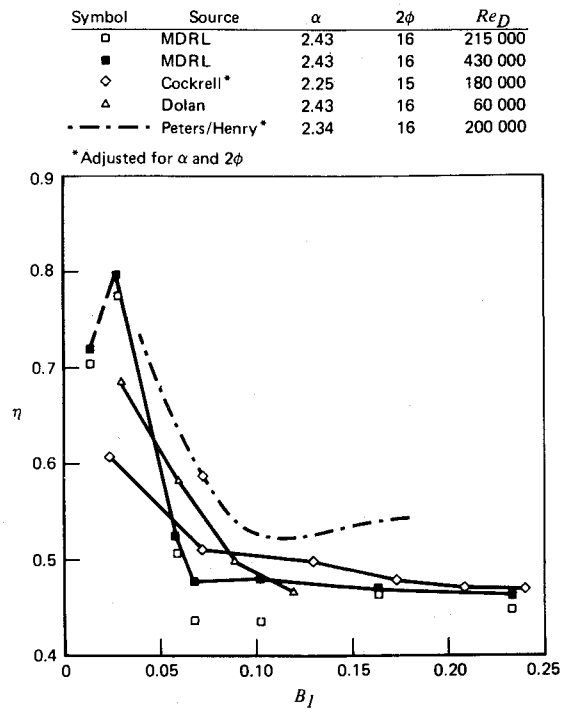

Fig. 11 Experimental effectiveness data as a function of inlet blockage for the 2.43/16 diffuser.

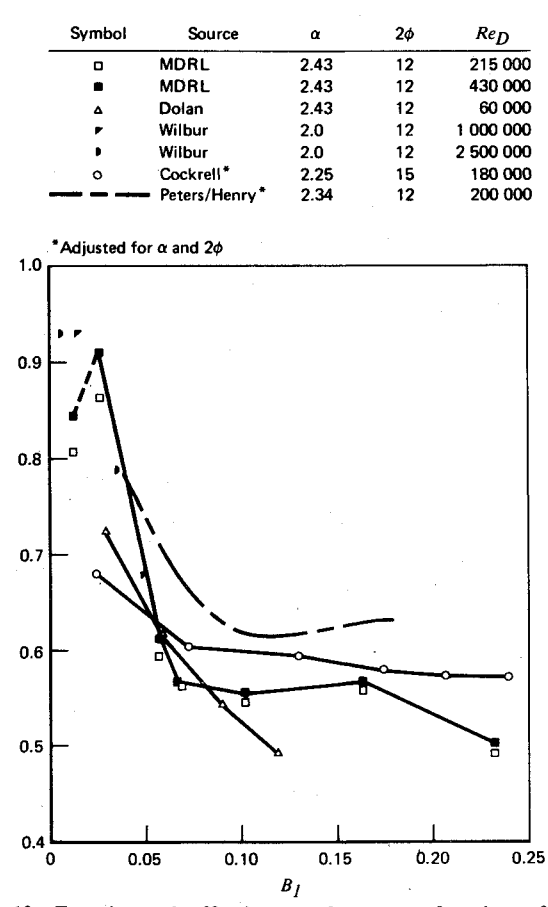

Fig. 12 Experimental effectiveness data as a function of inlet blockage for the 2.43/12 diffuser.

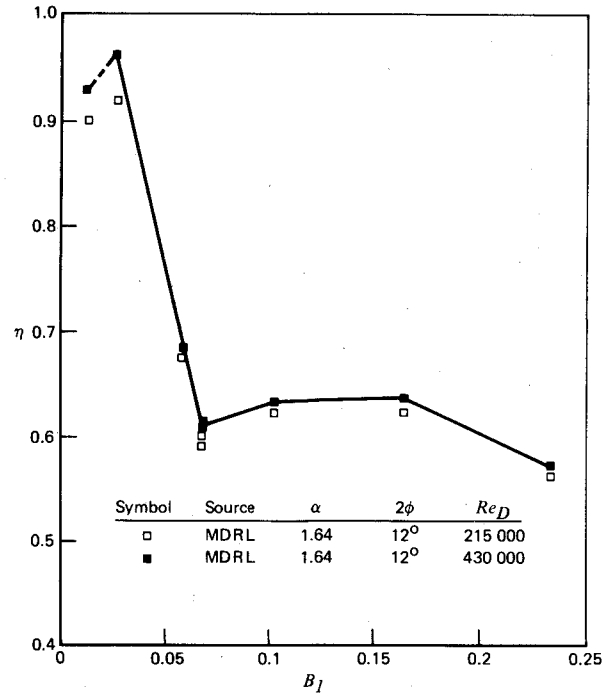

Fig. 13 Experimental effectiveness data as a function of inlet blockage for the 1.63/12 diffuser.

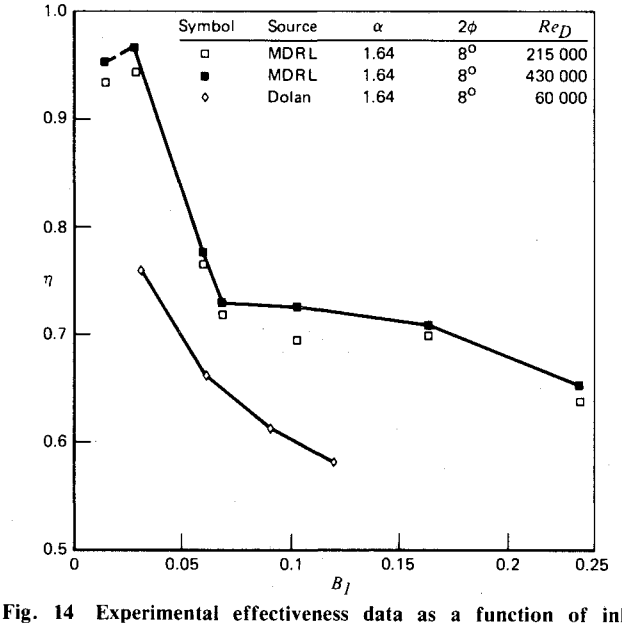

Fig. 14 Experimental effectiveness data as a function of inlet blockage for the 1.64/8 diffuser.

least inlet blockage specified; 6) axisymmetric inlet flow profiles with no inlet swirl; and 7) inlet conditions generated by natural boundary-layer growth.

Only four references[14-17] met these criteria; also, because of differences in geometry, some required interpolation or some adjustment for the comparison plots. Reference 14 provides empirical correlations, which also were used.

The comparisons with published data are made in terms of the effectiveness η, since no published data are available concerning exit distortion in terms of ψ_{x2}. A separate plot is given for each diffuser geometry.

Figure 11 shows the present data for the 2.43/16 diffuser, along with all comparable data found. The agreement with other sources is quite good; the deviation is of the same order as the differences among other investigators. The Dolan-Runstadler data[16] suggest a continued steep decline of η with blockage, but the present configuration was at the low area ratio end of their study, and some extrapolation was involved in their performance maps. In addition, their Reynolds numbers are lower by factors of about 4 and 8, respectively. Their definitions also differ, but the data are sufficient to compute η as defined by Eq. (1).

The dash-dot line is an empirical correlation proposed by Henry, Wood, and Wilbur,[14] based on experimental data with a single ratio of 2.2. The plotted curve was obtained by adjusting the Henry correlation according to the formula

$$1-\eta_{2.43}=(1-\eta_{2.2})\,(2.43/2.2)^{1.6} \tag{4}$$

where the subscripts of η refer to the respective area ratios. This formula was suggested by Henry et al.[14]

Figure 12 compares data for the 2.43/12 diffuser, with much the same comments and conclusions. Several additional data points are shown as solid symbols, taken from very careful and detailed measurements by Little and Wilbur.[15] These points confirm the general trends.

No comparable data were found for the 1.64/12 case (Fig. 13). The relatively poor performance at $B_I=0.068$ is consistent and repeatable but not understood. Figure 14 shows data for the 1.64/8 model. The Dolan-Runstadler curve[16] required considerable extrapolation of measured values and should not be weighted too heavily in this case.

Summary

The performance of four different diffusers was determined experimentally with seven different inlet velocity profiles for each diffuser, over a Reynolds number range of 100,000-700,000 at Mach numbers up to 0.3. Performance was evaluated in terms of static pressure recovery and exit distortion.

The effectiveness values measured with screen-generated inlet profiles agree with published data taken with naturally developed inlet boundary layers. The agreement is within the approximately 10% variation found among different investigators. Since the radial distributions of turbulence intensities were considerably different in the two cases, the findings suggest that the importance of this factor is secondary to the role of the mean velocity profile.

It is reasonable to conclude that the simulation of inlet profiles with screens should be an acceptable engineering procedure for axisymmetric diffusers whose configurations are reasonably close to those used in this investigation, when operated at comparable Reynolds and Mach numbers. Extrapolations of this conclusion to other geometric and flow conditions is tempting and may well be possible, but it cannot be made on the basis of the purely empirical approach followed here.

Exit distortion indices based on force measurement were determined in all cases and were found to be very sensitive to inlet blockage for small values of the latter. However, increases of inlet blockage beyond approximately 0.07 caused only minor increases of exit nonuniformity.

References

[1] Sajben, M., "Problems of Internal Fluid Mechanics," *Workshop on Prediction Methods of Jet V/STOL Propulsion Aerodynamics of the Naval Air Systems Command,* Arlington, Va., July 28-31, 1975.

[2] Sajben, M., Kroutil, J.C. Hoffman, G.H., and Sedrick, A.V., "Generation of Velocity Profile Using Screens of Nonuniform Solidity," *AIAA Journal,* Vol. 13, April 1975, pp. 417-418.

[3] Elder, J.W., "Steady Flow Through Nonuniform Gauzes of Arbitrary Shape," *Journal of Fluid Mechanics,* Vol. 5, April 1969, pp. 355-368.

[4] Livesay, J.L. and Laws, E.M., "Simulation of Velocity Profiles by Shaped Gauze Screens," *AIAA Journal,* Vol. 11, Feb. 1973, pp. 184-188.

[5] McCarthy, J.H., "Steady Flow Past Nonuniform Wire Grids," *Journal of Fluid Mechanics*, Vol. 19, 1964, pp. 491-512.

[6] Sajben, M., Kroutil, J.C., and Sedrick, A.V., "Performance and Exit Distortion of Diffusers as Determined by Force Measurements," *AIAA Journal,* Vol. 13, May 1975, pp. 547-512.

[7] Sajben, M., Chen, C.P., and Kroutil, J.C., "Comparison of Conventional and Force-Based Distortion Index Measurements," *AIAA Journal,* Vol. 14, Oct. 1976, pp. 1500-1501.

[8] Behrens, W., private communication, 1973, California Institute of Technology, Pasadena, Calif.

[9] Hinze, J.O., *Turbulence,* McGraw Hill, New York, 1959, p. 488, Figs. 7-10.

[10] Okwuobi, P.A.C. and Azad, R.S., "Turbulence in a Conical Diffuser with Fully Developed Flow at Entry," *Journal of Fluid Mechanics,* Vol. 57, Feb. 1973, pp. 603-622.

[11] Coles, D., "The Law of the Wake in the Turbulent Boundary Layer," *Journal of Fluid Mechanics,* Vol. 1, 1956, pp. 191-226.

[12] Hoffman, G.H., "Rotational Inviscid Flow in Axisymmetric Ducts," McDonnell Douglas Rept. MDC Q0472, Nov. 1972.

[13] Sharan, V.K., "Improving Diffuser Performance by Artifical Means," *AIAA Journal,* Vol. 10, Aug. 1972, pp. 1105-1107.

[14] Henry, J.R., Wood, C.C., and Wilbur, S.W., "Summary of Subsonic Diffuser Data," NACA RM L56F05, 1956.

[15] Little, B.H., Jr. and Wilbur, S.W., "Performance and Boundary Layer Data from 12° and 23° Conical Diffusers of Area Ratio 2.0 at Mach Numbers up to Choking and Reynolds Numbers up to 7.5×10^6," NACA Rept. 1201, 1954.

[16] Dolan, F.X. and Runstadler, P.W., Jr., "Pressure Recovery Performance of Conical Diffusers at High Subsonic Mach Numbers," Creare, Inc., Hanover, N.H., Rept. TN-165, 1973.

[17] Cockrell, D.J. and Markland, E., "A Review of Incompressible Diffuser Flow," *Aircraft Engineering,* Vol. 34, Oct. 1963, pp. 286-292.